

Transient Pauli blocking in a InN film as a mechanism for broadband ultrafast optical switching

Junjun Jia*

*Global Center for Science and Engineering (GCSE),
 Faculty of Science and Engineering, Waseda University,
 3-4-1 Okubo, Shinjuku, Tokyo 169-8555, Japan. and
 Graduate School of Advanced Science and Engineering,
 Waseda University, 3-4-1 Okubo, Shinjuku, Tokyo 169-8555, Japan*

Minseok Kim and Yuzo Shigesato

*Graduate School of Science and Engineering,
 Aoyama Gakuin University, Sagamihara,
 Kanagawa, 252-5258, Japan.*

Ryotaro Nakazawa

Institute for Molecular Science, 38, Nishigounaka, Myodaiji, Okazaki, Aichi, 444-8585, Japan

Keisuke Fukutani and Satoshi Kera

*Institute for Molecular Science, 38, Nishigounaka,
 Myodaiji, Okazaki, Aichi, 444-8585, Japan. and
 The Graduate University for Advanced Studies (SOKENDAI),
 Hayama-cho, Miura-gun, Kanagawa 240-0193, Japan.*

Toshiki Makimoto

*Graduate School of Advanced Science and Engineering,
 Waseda University, 3-4-1 Okubo, Shinjuku, Tokyo 169-8555, Japan*

Takashi Yagi

*National Metrology Institute of Japan (NMIJ),
 National Institute of Advanced Industrial Science and Technology (AIST),
 Central 5, 1-1-1 Higashi,
 Tsukuba, Ibaraki 305-8565, Japan
 (Dated: January 22, 2026)*

The transient Pauli blocking effect offers a promising route for achieving ultrafast optical switching in semiconductors, enabling a rapid switching from an initially opaque state to a relatively transparent state upon photoexcitation. Herein, we demonstrate broadband ultrafast optical switching in degenerate InN thin films, spanning the visible to near-infrared spectral range, using pump-probe transient transmittance measurements. To elucidate the underlying physical mechanism, we perform probe-energy-resolved analysis for ultrafast dynamics, and develop a theoretical model based on a quasi-equilibrium Fermi-Dirac distribution. The model successfully captures the experimental transients and yields an electron-phonon coupling constant of $1.0 \times 10^{17} \text{ W/m}^3 \cdot \text{K}$, along with an electronic specific heat coefficient ranging from 1.52 to 2.02 $\text{mJ/mol} \cdot \text{K}^2$, which allow direct prediction of the spectral switching window. Notably, we demonstrate that the Pauli blocking effect can be induced solely by a laser-excitation driven rise in electronic temperature, without requiring significant carrier injection into the conduction band in degenerate semiconductors. These findings offer new insights for designing ultrafast optical modulators, shutters, and photonic devices for next-generation communication and computing technologies.

I. INTRODUCTION

With the rapid advancement of high-intensity laser technology, integrating laser irradiation with materials, which can generate various nonequilibrium excitation states, has opened up new avenues for the design of func-

tional materials and devices [1, 2]. Since most commercial lasers operate at wavelengths extending up to the ultraviolet region, semiconductor materials have become ideal platforms for generating light-driven functionalities, such as optical switching devices [3], second- [4] or higher-order harmonic generation [5, 6], thereby enabling a wide range of emerging applications.

When semiconductors are irradiated with intense pulsed laser with photon energy exceeding the bandgap, a large number of electrons are excited from the va-

* jia@aoni.waseda.jp

lence band into the conduction band. These photoexcited electrons rapidly undergo energy and momentum relaxation owing to the fast electron-electron interaction, thermalizing from their initial non-thermal distribution to a quasi-equilibrium Fermi-Dirac (FD) distribution characterized by an elevated electronic temperature and then cools down mainly by electron-phonon scattering [7, 8], as illustrated in Fig. 1, which subsequently cools mainly via carrier-phonon scattering. Before recombining with holes left in the valence band, the thermalized electrons transiently occupy the conduction band on ultrafast timescales, ranging from femtoseconds to nanoseconds. This electronic occupation gives rise to a *transient Pauli blocking effect*, which blocks absorption of photons with energies at or slightly above the bandgap [2]. As a result, the material undergoes an ultrafast switching from an initial opaque to a transiently transparent state, significantly modulating its optical properties of the semiconductor on ultrafast timescales. Such an effect offers new opportunities to exploit the transient state as a novel functional phase for optical applications, including ultrafast optical switches, filters and modulator, as shown in Fig. 1.

How should we interpret the influence of *transient Pauli blocking effect* on the optical properties of semiconductors? Once the conduction band is populated with a thermalized electron gas, a notable modification to the optical response is expected from collective motion of these carriers. This behavior can be treated within the framework of classical Drude model. According to the Drude model, light with frequencies below the plasma frequency is reflected, while those with higher frequencies can propagate through the material [9, 10]. Photoexcitation-induced changes in carrier density can thus modulate the plasma frequency and, in turn, the optical properties of the material. However, even at high excited carrier density upto 10^{21} cm^{-3} , the collective response remains relatively weak in the visible spectrum, as those observed in heavily doped In_2O_3 films [11]. Therefore, this collective behavior is expected to manifest primarily in the near-infrared region and long-wavelength regions.

On the other hand, the transient occupation of thermalized electrons in the conduction band often leads to a temporary increase in transmittance in the visible region [1, 12], a phenomenon not adequately explained by the conventional Drude model. Due to its ultrafast and nonequilibrium nature, this behavior lies beyond the scope of classical optical transition theories developed under equilibrium assumptions [13]. Although advanced theoretical approaches, such as time-dependent density functional theory (TDDFT) [14, 15] are being actively explored in this field, a unified theory that incorporates direct/indirect optical transitions [13] with band gap renormalization [16] and the collective response of thermalized electrons and so on is still lacking. Moreover, the substantial computational cost of these methods hinders their practical use in interpreting experimental results

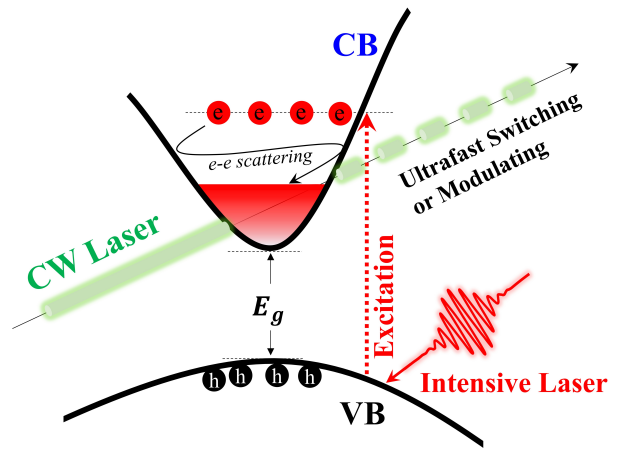


FIG. 1. **Schematic illustration of ultrafast optical switching in semiconductors via transient Pauli blocking.** Under intensive laser irradiation with photon energy exceeding the band gap E_g , electrons are excited into conduction band and rapidly thermalize through electron-electron scattering ($e-e$ scattering), forming a transient quasi-equilibrium Fermi-Dirac distribution. The resulting electronic occupation transiently blocks optical absorption, enabling an ultrafast switching from an opaque to a transparent state. This mechanism offers opportunities for laser pulse modulation and other advanced optical applications. CB: conduction band, VB: valence band.

from ultrafast spectroscopy. From an optical perspective, the transient occupation of thermalized electrons in the conduction band blocks previously allowed optical transitions, thereby reducing absorption and giving rise to a transient increase in transmittance. However, the physical origin of the *transient Pauli blocking effect* and its manifestation as a broad spectral feature in the visible range remains insufficiently understood [17, 18], highlighting the need for a more simplified theoretical framework.

In this study, we investigate the *transient Pauli blocking effect* in a degenerate wurtzite-structured InN film using pump-probe transient transmittance measurements with multicolor probe lasers, different from our previously reported degenerate pump-probe approaches [1]. We develop a theoretical model that captures the observed ultrafast electronic dynamics, and reveals a new physical origin of the *transient Pauli blocking effect*. Specifically, we find that *transient Pauli blocking effect* can be induced solely by a laser-excitation driven rise in electronic temperature, without requiring significant carrier injection into the conduction band. Moreover, our model defines the spectral window over which optical switching occurs. This framework not only deepens fundamental understanding of nonequilibrium carrier dynamics including its measurement, but also opens new avenues for realizing semiconductor-based ultrafast optical switches, filter and modulators leveraging *transient*

Pauli blocking effect as an active control mechanism.

II. EXPERIMENTAL AND COMPUTATIONAL DETAILS

Molecular epitaxial evaporation was used to grow the *c*-oriented InN film on a *c*-sapphire substrate. The fabricated InN sample is polycrystalline *n* type, with an electron concentration of $5.50 \pm 0.82 \times 10^{19} \text{ cm}^{-3}$ and a Hall mobility of $5.43 \pm 0.64 \text{ cm}^2/\text{Vs}$ using a HL-5500PC Hall measurement system (Bio-Rad). The film thickness was determined to be 400 nm by fitting the Fourier-transform infrared (FTIR) spectrum using the Drude model. The out-of-plane lattice constants *c*, calculated from the X-ray diffraction (XRD) (002) peak at $2\theta=31.36172^\circ$, was found to be 5.700 Å, in good agreement with the standard powder diffraction value of 5.7033 Å at room temperature [19, 20]. The absorption coefficient α was extracted from optical transmittance (*T*) and reflectance (*R*) spectra measured using a UV-Vis-NIR spectrometer (UV-3600 plus, Shimadzu, Japan), based on the relation $T = (1 - R) \exp(-\alpha d)$, where *d* is the film thickness.

High-sensitivity ultraviolet photoelectron spectroscopy (HS-UPS) was performed to determine the electronic structure around the top of valence band for the used InN film at the Institute for Molecular Science. The base pressure during the measurements was approximately 10^{-8} Pa . A bias voltage of -5 V was applied to the sample. A monochromatic Xe I α line (photon energy: 8.437 eV) was used as the excitation source. The light incident angle was 45° with respect to the sample surface. The HS-UPS measurements were performed using the hemispherical analyzer (MBS A-1) in the normal emission geometry, where the sample's surface-normal was aligned along the analyzer axis, and the pass energy was set to 10 eV. The total energy resolution was set to 75 meV. The photoelectrons' kinetic energy at the Fermi level and the instrumental energy resolution were calibrated using the Fermi edge of a gold film measured at room temperature.

Femtosecond time-resolved transient transmission measurements were conducted using a pump-probe technique to investigate ultrafast carrier dynamics. The InN film was excited at room temperature by a 140 fs Ti:Sapphire laser pulse (Repetition rate: 76 MHz, photon energy: 1.55 eV). The laser beam was split using a polarized beam splitter: the majority of the power was directed to the sample as the pump, while the remaining power was coupled into a supercontinuum generation module (FemtoWHITE 800, NKT Photonics) to produce the broadband probe laser spanning 400–1000 nm. Both pump and probe beams were focused normal to the sample surface (incident angle: 90°) using a $10\times$ objective lens (Mitutoyo). The pump beam spot diameter ($1/e^2$ diameter) was $10.3 \mu\text{m}$ as determined by the knife-edge method. The transmitted probe light was spectrally resolved using a grating spectrometer and subsequently de-

tected by a silicon photodetector (2107-FC, New Focus).

To interpret the ultrafast dynamics observed in the transient transmission measurements, the photoexcited carrier density (n_{ex}) was estimated using the method proposed by J. Menéndez *et al.* [21], which accounts for the lateral diffusion of excited electrons during pumping. In this estimation, the room-temperature average carrier lifetime was conservatively set to 5 ps based on our pump-probe measurements, the carrier diffusion coefficient was taken as $0.14 \text{ cm}^2/\text{s}$ derived from the measured Hall mobility, and the surface recombination velocity was assumed to be $2 \times 10^7 \text{ cm/s}$. For a pumping power of 220 mW at 1.55 eV, n_{ex} was estimated to be $3.84 \times 10^{16} \text{ cm}^{-3}$, for which the measured $R=0.136$ and $\alpha=29346 \text{ cm}^{-1}$ were used.

Density functional theory (DFT) calculations were performed using the Vienna *ab initio* Simulation Package [22] with the projector augmented-wave method [23]. The experimentally measured lattice constants were used, while keeping the fractional coordinates fixed, to calculate the band structure of wurtzite InN (space group No. 186, $P6_3mc$) using the Heyd-Scuseria-Ernzerhof (HSE06) hybrid exchange correlation functional with a plane-wave cutoff of 400 eV. The spin-orbit coupling effect was included to accurately capture the valence band splitting. Optical transition matrix elements were calculated in the longitudinal gauge [24]. They are given as matrix elements $\langle c\mathbf{k}|\mathbf{p}|v\mathbf{k}\rangle$ of the momentum operator \mathbf{p} between the conduction band *c* and the valence band *v* at a given \mathbf{k} point. Considering the spin-orbit degenerate states $i, j=1, 2$ in the conduction and valence bands, the magnitude of matrix elements for direct transitions can be expressed as

$$|\mathbf{M}_{cv}| = \sum_{c_i, v_j} \langle c_i \mathbf{k} | \mathbf{p} | v_j \mathbf{k} \rangle. \quad (1)$$

Then, the transition probability can be proportional to the optical matrix element, namely $p_{cv} \propto |\mathbf{M}_{cv}|^2$.

III. RESULTS AND DISCUSSION

To elucidate the *transient Pauli blocking effect* in InN within the frame of band theory, we started by calculating the band structure of wurtzite-structured InN using the HSE06 functional, incorporating spin-orbit coupling effect to account for valence band splitting. The calculation was performed using experimentally determined lattice constants ($a=3.533 \text{ \AA}$ and $c=5.700 \text{ \AA}$) at room temperature. The calculated band structure is shown in Fig. 2(a), revealing a band gap of 0.79 eV at the Γ point. This value is in good agreement with previous theoretical calculations [25] and the experimentally measured band gap of $\sim 0.80 \text{ eV}$ obtained from PL measurements on low-carrier-concentration InN sample [26]. Given its degenerate nature of the used InN sample, arising from its high electron concentration, the position of

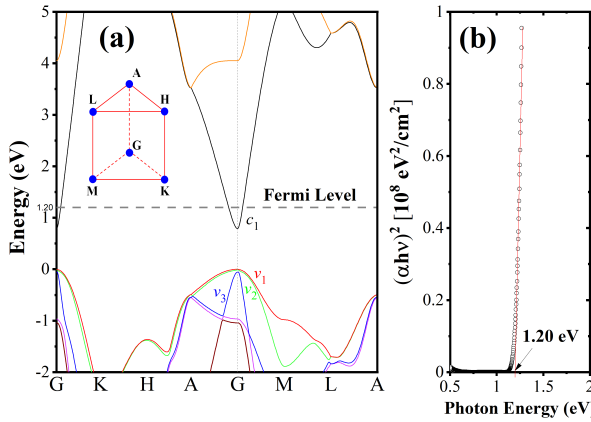


FIG. 2. **Electronic band structure and optical band gap of wurtzite InN.** (a) Calculated band structure of wurtzite InN using the HSE hybrid functional with spin-orbit coupling interaction included. The inset shows the high-symmetry points in the first Brillouin zone. The dashed line represents the Fermi level, estimated based on the unintentional carrier density obtained from Hall effect measurements. (b) Tauc plot used to extract the optical band gap from the experimental data (shown as circles).

Fermi level was estimated based on the Burstein–Moss effect [27]. The corresponding Fermi level shift (ΔE) is calculated by

$$\Delta E = \frac{\hbar^2}{2m_e^*} (3\pi^2 n_0)^{\frac{2}{3}}, \quad (2)$$

where \hbar is the reduced Planck constant, m_e^* is the electron effective mass, and n_0 is the electron concentration. Because the $\mathbf{k} \cdot \mathbf{p}$ interaction across the narrow direct gap of InN causes strong nonparabolic E - k dispersion in the CB [28, 29], an increased m_e^* away from the CB minimum must be taken into account [1, 29, 30]. For a carrier density of $5.50 \times 10^{19} \text{ cm}^{-3}$, m_e^* is estimated to be $0.13m_0$, where m_0 is the free electron mass, resulting in a Fermi level shift of approximately 0.40 eV. Consequently, the effective optical band gap is estimated to be 1.19 eV. This value is in close agreement with the optical band gap extracted from Tauc’s plot in Fig. 2(b).

To further determine the Fermi level, the HS–UPS spectrum of the InN thin film was collected, as shown in Fig. 3. The horizontal axis indicates the energy relative to the Fermi level, and the vertical axis represents the intensity of the photoelectrons. On a logarithmic scale, a weak but continuous signal can be observed up to 0 eV. A change in the spectral slope appears around -1.2 eV, which is assigned to the valence band maximum (VBM). The electronic states observed between the VBM and the Fermi level arise from in-gap states and electrons occupying the conduction band. The line shape near 0 eV is well reproduced by a FD distribution, indicating partial occupation of the conduction band. Because the InN film is degenerate, the energy difference between the Fermi level

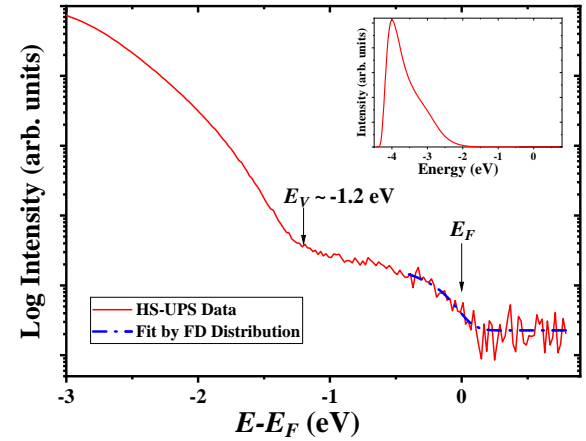


FIG. 3. **HS–UPS spectrum of the InN thin film.** HS–UPS spectrum obtained using the monochromatic Xe I α line (photon energy of 8.437 eV), plotted on a logarithmic scale. The dash-dotted line near 0 eV represents the fitting curve based on the FD distribution. The inset shows the same spectrum on a linear scale. The labels “ E ”, “ E_F ”, and “ E_V ” indicate the energy, Fermi level, and the valence band maximum, respectively.

and the VBM corresponds approximately to the optical band gap, consistent with the value obtained from the Tauc plot in Fig. 2(b).

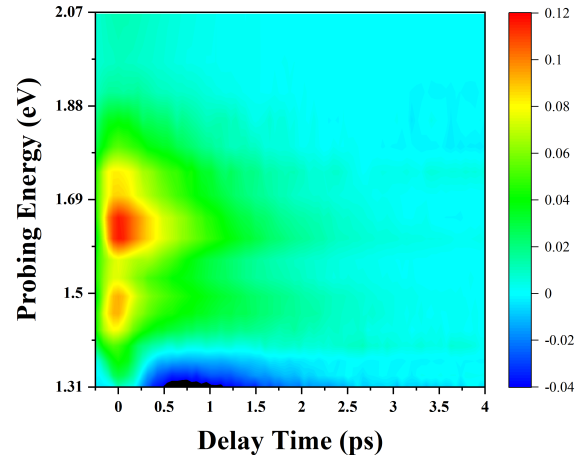


FIG. 4. **Time-resolved transient transmittance spectra of InN.** Transient transmittance spectra measured at a pump fluence of 63.8 J/m^2 , using a pump laser with photon energy of 1.55 eV. The probe photon energies range from 1.31 to 2.07 eV.

Optical Switching: Figure 4 shows that transient transmittance spectrum measured across the probe energy range of 1.31–2.07 eV under optical excitation at

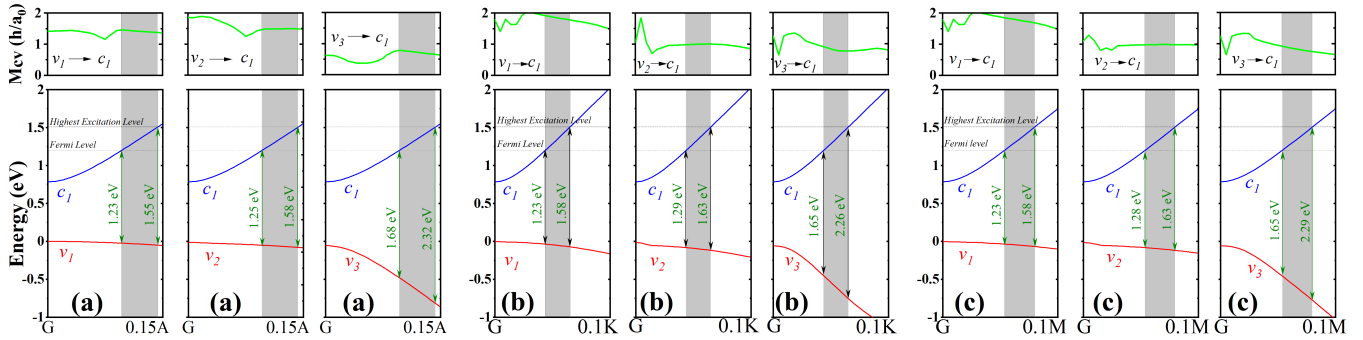


FIG. 5. **Band structures and optical transition matrix elements of wurtzite InN.** Band structures illustrating possible optical transitions from the valence bands (v_1 , v_2 , and v_3) to the lowest conduction band c_1 along three high-symmetrical paths ((a): $\Gamma \rightarrow A$, (b): $\Gamma \rightarrow K$, and (c): $\Gamma \rightarrow M$). The upper panels show the corresponding optical matrix elements, which are proportional to the transition probability. The dash-dotted lines denote the highest excitation level provided by a 1.55 eV pump laser, while the dotted lines indicate the Fermi level at equilibrium before photoexcitation. Shaded gray regions represent the energy window accessible to the probe light.

1.55 eV with a pump fluence of 63.8 J/m^2 . The transient transmittance signal is defined as $dT/T = [T(t) - T(0)]/T(0)$, where $T(t)$ and $T(0)$ represent the time-dependent and static transmittance, respectively. The overall temporal response shows two notable switching regions, suggesting the potential of InN as a multicolored optical switching material, where “multicolor” refers to distinct optical response at multiple probe photon energies. The most pronounced switching region is centered at approximately 1.63 eV, while another switching region is located at around 1.43 eV. These switching states are attributed to *transient Pauli blocking effect*, which induces a reversible switching from an opaque to a relatively transparent state [2]. The underlying mechanism can be interpreted by considering the allowed optical transition pathways from different valence bands to the lowest-lying conduction band (c_1), as shown in Fig. 2(a).

From the perspective of the pump-probing measurement principle, when electrons are excited and injected into the conduction band by the pump laser, the probe laser can detect their transient occupancy. Based on the calculated band structure, we evaluated the optical transition probability from the valence bands to the conduction band, which help to explain the optical switching behavior observed in Fig. 4. The possible interband transitions near the Γ point are illustrated in the upper panels of Figs. 5, where optical transitions from $v_1 \rightarrow c_1$, $v_2 \rightarrow c_1$, and $v_3 \rightarrow c_1$ are all dipole-allowed. Taking into account the highest excitation level provided by the 1.55 eV pump laser and the estimated static Fermi level at 1.20 eV, a broad transient transmission window ranging from 1.23 to 2.32 eV is expected, as shown in Fig. 5. This range is in rough agreement with the experimentally observed dT/T spectrum from 1.31 to 2.07 eV in Fig. 4. A more quantitative interpretation, however, requires incorporating the thermal broadening of the Fermi-Dirac distribution at elevated electron temperature, which will be discussed in the final section.

The emergence of two distinct optical switching centers can be attributed to the presence of multiple allowed optical transition pathways between the valence and conduction bands. For a given photon energy, the final conduction-band state may be accessed via more than one interband transition channel. The switching feature centered at 1.43 eV is primarily associated with optical transitions from the $v_1 \rightarrow c_1$ and $v_2 \rightarrow c_1$ bands, both of which exhibit high optical transition probability (M_{cv}), as shown in Fig. 5. The higher-energy switching feature near 1.63 eV is attributed to optical transitions from the $v_2 \rightarrow c_1$ and $v_3 \rightarrow c_1$ bands. Notably, transient transmission persists even above 1.70 eV in Fig. 4, exceeding the pump photon energy of 1.55 eV, which is attributed to the $v_3 \rightarrow c_1$ transition. These observations confirm that the *transient Pauli blocking effect* enables broadband optical switching, spanning a spectral range

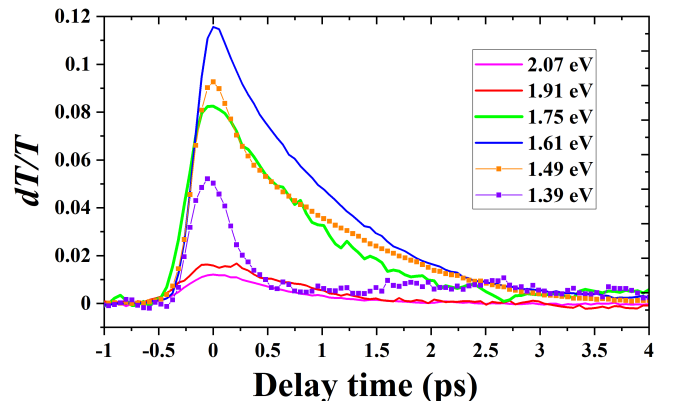


FIG. 6. **Energy-resolved transient transmittance dynamics in InN.** Transient dT/T traces measured under 1.55 eV excitation at a pump fluence of 63.8 J/m^2 , with the probing energy systematically varied to capture energy-dependent carrier dynamics.

wider than the excitation energy.

It is also worth noting that a negative signal appears around 1.31 eV for delays starting from approximately 0.25 ps. This feature is attributed to absorption arising from optical transitions between the valence band and the conduction band states near Fermi level. After photoexcitation, some electrons close to the Fermi level are thermalized to higher energies through scattering processes, leaving behind empty states (“hole”) close to the Fermi level. These empty states allow additional optical transitions of photoexcited electrons, i.e., absorption, resulting in the negative feature observed in the dT/T traces.

Transient Transmittance Trace: Fig. 6 presents the dT/T traces measured at different probe photon energies. The dependence of the peak dT/T intensity on probe energy is consistent with the contour map shown in Fig. 4. All traces exhibit a rapid rise to a maximum followed by a subsequent decay. The initial rise is commonly attributed to the rapid population of the conduction band states by thermalized electrons via electron-electron scattering processes [8], after which the thermalized electrons gradually recombine with holes in the valence band. However, the total photoexcited electron density in our experiment is estimated to be only $3.84 \times 10^{16} \text{ cm}^{-3}$, which is insufficient to directly induce a broadband Pauli blocking effect. We therefore hypothesize that the energy of the photoexcited electrons transferred to the conduction electrons through energy and momentum relaxation, forming a “hot” thermalized FD distribution. Under this assumption, the observed dT/T signal at a given probe energy reflects the temporal evolution of the electronic occupation, namely the cooling dynamics of the “hot” thermalized FD distribution.

For an isotropic parabolic band dispersion, a given transition energy (e.g., the probe photon energy 1.55 eV) corresponds to a single or only a few k -points in k -space. When the bands are anisotropic, however, the situation becomes more complex. For instance, in diamond structured Ge, the energy separation between the valence and conduction bands remains nearly constant over a range of k -values along the (111) direction, leading to an extreme case where the interband critical point is two-dimensional in character [31]. In contrast, for wurtzite InN, the effective electron mass parallel ($m_{||}=0.068m_0$) and perpendicular ($m_{\perp}=0.070m_0$) to the c direction [32] are nearly identical, indicating only a modest anisotropy in its electronic band structure. Therefore, a given transition energy in InN is expected to involve electronic states at a single (or a few) k -points, rather than an extended k -space region.

On the other hand, at a fixed photon energy, the final conduction-band states involved in the optical transition can still couple to multiple valence-band states, as illustrated in Fig. 5. For instance, despite the relatively small energy separation between the v_1 and v_2 valence bands, a given probe photon energy may excite transitions from both $v_1 \rightarrow c_1$ and $v_2 \rightarrow c_1$, leading to the

detection of different conduction band states above the static Fermi level, as illustrated in Fig. 5. Consequently, the measured dT/T traces may reflect carrier thermalization dynamics across multiple energy levels. This effect is particularly evident for probe energies below 1.49 eV, where both $v_1 \rightarrow c_1$ and $v_2 \rightarrow c_1$ transitions are allowed and the transient traces exhibit pronounced bi- or multi-exponential decay features, as shown in Fig. 6. To avoid overinterpretation of the dT/T traces that may involve multiple optical transitions, we focused on those measured at probe energies above 1.61 eV, where the signal predominantly originates from the $v_3 \rightarrow c_1$ transition. Although slight variations still exist among different k -space directions (e.g., $\Gamma \rightarrow A$, $\Gamma \rightarrow K$, and $\Gamma \rightarrow M$), the corresponding transitions at a given probe energy can be reasonably approximated by a single dominant channel owing to their small energy separations.

To extract the characteristic cooling time of “hot” thermalized FD distribution, the dT/T traces were first fitted using a simple exponential relaxation function: $dN/dt = G(t) - N/\tau$, where N is the number of thermalized electron contributing to the signal at the probe level, and τ represents the characteristic cooling time. The generation term, $G(t) \propto \exp[-2(t/t_p)^2]$, describes carrier injection induced by a Gaussian pump pulse with the pulse width t_p . For probe photon energies below 1.49 eV in Fig. 6, the dT/T traces exhibit bi- or multi-exponential characteristics, likely due to overlapping contributions from multiple optical transitions. In contrast, for probe photon energies above 1.75 eV in Fig. 6, a single exponential fit adequately reproduces the measured dynamics. Notably, as the probe energy increases from 1.75 to 2.07 eV, the extracted τ gradually decreases from 0.90 ps to 0.66 ps, which are slightly smaller than the previously reported characteristic times [17, 33, 34]. This trend indicates that higher probe photon energies correspond to higher-energy states within the hot thermalized FD distribution, where carrier cooling proceeds more rapidly. Such an energy dependence suggests that the cooling dynamics are primarily governed by energy relaxation through electron-phonon coupling, and that a more accurate description, accounting for the energy-dependent nature of the electron distribution, is required to model the cooling dynamics of the thermalized FD distribution.

To further elucidate the cooling mechanism, we quantitatively evaluated the influence of defect-induced momentum scattering using the measured mobility. The InN film used in this study exhibited a mobility of $\mu=5.43 \text{ cm}^2/\text{Vs}$. The average scattering time τ_s during transport can be estimated from $\mu=e\tau_s/m_e^*$, where e is the elementary charge. Taking $m_e^*=0.13m_0$, the calculated average scattering time is approximately 0.40 fs. This value is much shorter than the typical thermalization time on the order of picoseconds, indicating that momentum randomization caused by defect-related scattering, such as ionized impurity scattering [9], occurs much faster than energy redistribution. Consequently, such scatter-

ing mainly affects momentum relaxation but has only a limited impact on the overall carrier thermalization dynamics.

Modeling the cooling of the FD distribution: The cooling process of a hot thermalized FD distribution is primarily governed by electron–phonon interactions, which can be effectively described by the classical two-temperature model. Assuming that the electron–electron and phonon–phonon interactions are sufficiently fast to maintain local equilibrium within the carrier and phonon populations, the temporal evolution of the electron temperature T_e and the lattice temperature T_l can be described by evaluating the electron energy loss rate to the lattice using the Boltzmann equation [35], resulting in the two-temperature model [36, 37]

$$\begin{cases} C_e(T_e) \frac{\partial T_e}{\partial t} = I(t) - g_{ep}(T_e - T_l), \\ C_l \frac{\partial T_l}{\partial t} = g_{ep}(T_e - T_l), \end{cases} \quad (3)$$

where C_e (C_l) is the heat capacity of electrons (lattice), g_{ep} is the electron–phonon coupling coefficient. For InN, its heat capacity is $C_{\text{InN}}=2.197 \times 10^6 \text{ Jm}^{-3}\text{K}^{-1}$ [38]. For electronic temperatures below a few thousand Kelvin, a linear dependence of the electronic heat capacity, $C_e(T_e)=\gamma T_e$, has been found to be a good estimation [39]. The temporal evolution of laser intensity is given as [40, 41]

$$I(t) = \sqrt{\frac{\beta}{\pi}} \frac{AI_0}{t_p} \exp \left[-\beta \left(\frac{t - 2t_p}{t_p} \right)^2 \right], \quad (4)$$

where $\beta = 4\ln(2)$, I_0 is the pumping fluence, $A = (1 - R)(1 - e^{-\alpha d})$ is the effective absorption coefficient. Note that we neglect thermal diffusion processes in Eqs. (3).

The cooling of the electron temperature leads to a gradual narrowing of the FD distribution from its thermally broadened profile. From the aspect of the pump-probe measurement, the temporal evolution of occupation probability of electrons at a given energy level (E_p) in the conduction band for degenerate semiconductors can be described by the following FD distribution

$$f(E_p) = \frac{1}{\exp\left(\frac{E_p - E_f(t)}{k_B T_e(t)}\right) + 1}, \quad (5)$$

where k_B is the Boltzmann constant and $E_f(t)$ denotes the time-dependent Fermi level, which evolves due to changes in the electronic temperature and the photoexcited carrier density in the conduction band. The electron population at E_p can then be expressed as

$$n_p(t) = \int_{E_p}^{E_p + \delta E} f(E_p, E_f(t), T_e(t)) \cdot D(E_p) dE, \quad (6)$$

where δE represents a small energy interval around E_p , corresponding to the energy width of the probe laser, and $D(E_p)$ is the density of states at energy E_p . Taking into account the nonparabolic nature of conduction band in InN, the E – k dispersion can be approximated by retaining the second-order k^2 ellipsoidal energy surfaces and introducing a nonlinear dependence on the energy, namely,

$$\frac{\hbar^2 k^2}{2m_0^*} = \gamma(E) = E + \alpha E^2 + \beta E^3 + \dots, \quad (7)$$

where m_0^* is the electron effective mass at the conduction band minimum, α and β are the nonparabolicity coefficients of the conduction band, E is the electron energy relative to the conduction band minimum (CBM). By keeping only the first nonlinear term, the well-known Kane quasilinear dispersion relation is obtained [28]:

$$\frac{\hbar^2 k^2}{2m_0^*} = E(1 + \alpha E). \quad (8)$$

From Eq. (8), the E – k dispersion can be obtained, and then the nonparabolic $D(E)$ can be derived as follow:

$$D(E) = \frac{1}{2\pi^2} \left(\frac{2m_0^*}{\hbar^2} \right)^{3/2} \sqrt{E(1 + \alpha E)} \cdot (1 + 2\alpha E). \quad (9)$$

Our simulation shows that $\alpha=0.20 \text{ eV}^{-1}$ accurately reproduces the Fermi level shift in the InN film under investigation.

Eq. (6) describes the time dependence of $n_p(t)$ at the probing level, which results from the evolution of the electron temperature $T_e(t)$ and $E_f(t)$ during the cooling process. From the aspect of the Pauli blocking effect, this quantity is considered proportional to the measured dT/T intensity. However, solving Eq. (6) requires accurately determining $E_f(t)$, which depends on both the electron temperature and the electron concentration in the conduction band. For a known electron density $n_{\text{total}}(t)$ at time t , $E_f(t)$ can be determined using a numerical bisection root-finding approach applied to the following equation

$$n_{\text{total}}(t) = \int_{E_c}^{\infty} f(E, E_f(t), T_e(t)) \cdot D(E) dE, \quad (10)$$

where $n_{\text{total}}(t) = n_0 + n_{\text{ex}}(t)$. Because $n_{\text{ex}} = 3.84 \times 10^{16} \text{ cm}^{-3}$ is three orders of magnitude smaller than n_0 , its contribution to $E_f(t)$ is negligible. Therefore, we assume $n_{\text{total}}(t) = n_0$. Under this condition, the Fermi level $E_f(t)$ can be determined self-consistently from the electron temperature $T_e(t)$ through the carrier-density conservation.

Following the above model, the temporal evolution of $n_p(t)$ at the probing level E_p can be obtained by first calculating $T_e(t)$ in Eq. (3) with an assumed set of parameters (g_{ep} and γ) using the fourth order Runge–Kutta

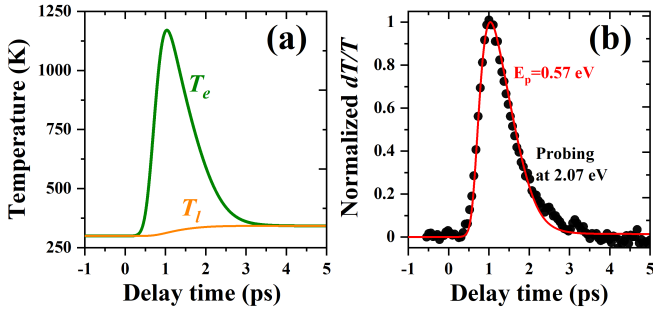


FIG. 7. **Comparison between calculated and measured carrier dynamics.** (a) Calculated temporal evolution of electron (T_e) and lattice (T_l) temperature, using $g_{ep} = 1.0 \times 10^{17} \text{ W/m}^3\cdot\text{K}$ and $\gamma = 1.52 \text{ mJ/mol}\cdot\text{K}^2$. (b) Experimental dT/T data (circular markers) obtained under 1.55 eV excitation with a pump fluence of 63.8 J/m^2 , probed at 2.07 eV. The solid line represents the calculated temporal evolution of electron occupation at $E_p=0.57 \text{ eV}$ above the CBM.

method. Then, $E_f(t)$ is determined self-consistently from $T_e(t)$ using Eq. (10). Finally, $n_p(t)$ is calculated based on Eq. (6). Since $n_p(t)$ directly reflects the experimentally measured dT/T traces, we compared the calculated $n_p(t)$ with the measured dT/T traces, which are mainly governed by approximately single-pathway optical processes corresponding to the $v_3 \rightarrow c_1$ transition. We found that using an approximately constant $g_{ep}=1.0 \times 10^{17} \text{ W/m}^3\cdot\text{K}$ and an electronic heat capacity coefficient γ in the range of 1.52 to 2.02 mJ/mol·K 2 can qualitatively reproduce the shape of the experimental dT/T traces. The best agreement is then achieved by tuning E_p with a slight adjustment of γ . The obtained E_p values systematically increases with increasing the probing energy. Note that in Eq. (5), E_p is defined as the energy separation between the probed final state in the conduction band and the CBM, whereas the probing energy in the experiments corresponds to the optical transition from the valence band to the conduction band. For the $v_3 \rightarrow c_1$ transition in InN, the c_1 band energy increases with the wavevector k , while the v_3 energy decreases. Therefore, a higher probing energy corresponds to a higher final state energy above the CBM, i.e., a larger E_p .

Fig. 7 presents a representative comparison between calculation and experiment. Fig. 7(a) shows the calculated temporal evolution of the electron and lattice temperatures, T_e and T_l , at $E_p=0.57 \text{ eV}$ above the conduction band minimum, using $g_{ep} = 1.0 \times 10^{17} \text{ W/m}^3\cdot\text{K}$ and $\gamma = 1.52 \text{ mJ/mol}\cdot\text{K}^2$. Fig. 7(b) compared the experimentally measured traces probed at 2.07 eV with the calculated dT/T trace at $E_p=0.57 \text{ eV}$ above the conduction-band minimum. The close agreement between them confirms that the model successfully captures the underlying dynamics of the dT/T response. It should be mentioned that both g_{ep} and γ were treated as effective fitting parameters within the two-temperature model. An approximately constant g_{ep} successfully reproduces all

measured transient transmittance traces. Given the lack of reported g_{ep} values for InN, we adopted $1.0 \times 10^{17} \text{ W/m}^3\cdot\text{K}$, which lies within the range commonly reported for metals such as aluminum ($2.45 \times 10^{17} \text{ W/m}^3\cdot\text{K}$) [42] and copper ($1.00 \times 10^{17} \text{ W/m}^3\cdot\text{K}$) [43]. Moreover, a γ value in the range of 1.52 to 2.02 mJ/mol·K 2 yields excellent agreement with the experimental transient data under femtosecond laser excitation. This value is comparable to those measured in metals such as Al or In [44]. The theoretical value, estimated from

$$\gamma = \frac{\pi^2 k_B^2}{3} D(E_F) \quad (11)$$

where $D(E_F)$ denotes the density of state at the Fermi level (0.40 eV) in equilibrium, is only 0.0064 mJ/mol·K 2 , reflecting the intrinsically low density of states in InN even when the Fermi level is relatively high. Such a large discrepancy should be understood in terms of the fundamentally different origin of the electronic excitation. In our case, the energy is stored in the hot FD distribution generated by femtosecond photoexcitation, where a significant portion resides in the high-energy tail above the Fermi level. This contrasts sharply with thermal excitation under equilibrium conditions, in which the carrier energy is primarily concentrated near the Fermi level. Therefore, the experimentally extracted γ represents a non-equilibrium contribution of photoexcited carriers and should not be directly compared with values derived from static low-temperature measurements.

Finally, we highlight several key implications of our findings. Our results demonstrate that the *transient Pauli blocking effect* can be effectively induced by a laser-driven rise in electronic temperature as shown in Fig. 7(a), rather than by the injection of a large number of electrons into the conduction band [2]. Our experiments further indicate that directly extracting thermalization or cooling times by fitting the transient transmittance traces with single- or multi-exponential functions may lead to misinterpretation, and that the underlying physical mechanisms must be carefully examined. Importantly, the theoretical framework based on a quasi-equilibrium Fermi-Dirac distribution proposed here provides a unified description of optical switching arising from *transient Pauli blocking effect*, and enables direct evaluation of the corresponding spectral switching range. These fundamental insights offer practical guidance for the laser-driven design of ultrafast optical switching devices, paving the way for next-generation photonic technologies such as all-optical communication and quantum information processing.

IV. CONCLUSIONS

In this study, we explore ultrafast optical switching in InN thin films using pump-probe transient transmittance measurement, combined with first-principles electronic band structure calculations. By resolving the transient

optical response across a range of probe photon energies, we disentangle the contributions of multiple interband transition pathways from the valence bands to the lowest lying conduction band. Moreover, our results reveal that conventional exponential fitting models often misinterpret the electron cooling dynamics, primarily due to the different cooling time at different probing level.

To gain deeper physical insights, we establish a theoretical framework based on a quasi-equilibrium FD distribution, which enables quantitative reproduction of the transient transmittance traces. We show that the observed ultrafast dynamics can be accurately described by a thermalized FD distribution with an elevated temperature, allowing precise prediction of transient optical transparency windows. Based on the experimen-

tal results, we further extract an electron–phonon coupling constant of $g_{ep}=1.0 \times 10^{17} \text{ W/m}^3\cdot\text{K}$, and an electronic specific heat coefficient in the range of 1.52 to 2.02 $\text{mJ/mol}\cdot\text{K}^2$ for InN.

Crucially, we demonstrate that the *transient Pauli blocking effect* can arise from a temperature-induced redistribution of electrons within the conduction band due to laser excitation, rather than from the injection of a large number of electrons. These findings provide a refined understanding of non-equilibrium carrier dynamics in semiconductors and opens new avenues for laser-driven material design of ultrafast optical switching components, including modulators, filters, and shutters for next-generation photonic applications such as all-optical networking or optical computing.

[1] J. Jia, T. Yagi, M. Mizutani, N. Yamada, T. Makimoto, Revealing the simultaneous increase in transient transmission and reflectivity in InN, *J. Appl. Phys.* **132**, 165702 (2022).

[2] J. Jia, H. Almossalami, H. Ye, N. Yamada, T. Yagi, Multivalley optical switching in germanium, *Phys. Rev. Applied* **23**, 024060 (2025).

[3] F. Schlaepfer, M. Lucchini, S. A. Sato, M. Volkov, L. Kasmi, N. Hartmann, A. Rubio, L. Gallmann, and U. Keller, Attosecond optical-field-enhanced carrier injection into the GaAs conduction band, *Nature Physics* **14**, 560 (2018).

[4] M. Lafrentz, D. Brunne, A. V. Rodina, V. V. Pavlov, R. V. Pisarev, D. R. Yakovlev, A. Bakin, and M. Bayer, Second-harmonic generation spectroscopy of excitons in ZnO, *Phys. Rev. B* **88**, 235207 (2013).

[5] H. Liu, Y. Li, Y. S. You, S. Ghimire, T. F. Heinz, D. A. Reis, High-harmonic generation from an atomically thin semiconductor, *Nature Physics* **13**, 262 (2017).

[6] D. Freeman, S. Yamada, A. Yamada, A. Kheifets, and K. Yabana, High order harmonic generation in semiconductors driven at near- and mid-IR wavelengths, *Phys. Rev. B* **106**, 075202 (2022).

[7] P. B. Allen, Theory of thermal relaxation of electrons in metals, *Phys. Rev. Lett.* **59**, 1460 (1987).

[8] A. Crepaldi, B. Ressel, F. Cilento, M. Zacchigna, C. Grazioli, H. Berger, Ph. Bugnon, K. Kern, M. Grioni, and F. Parmigiani, Ultrafast photodoping and effective Fermi–Dirac distribution of the Dirac particles in Bi_2Se_3 , *Phys. Rev. B* **86**, 205133 (2012).

[9] J. Jia, A. Yoshimura, Y. Kagoya, N. Oka, Y. Shigesato, Transparent conductive Al and Ga doped ZnO films deposited using off-axis sputtering, *Thin Solid Films* **559**, 69 (2014).

[10] J. Jia, T. Sugane, S. Nakamura, Y. Shigesato, p -type conduction mechanism in continuously varied non-stoichiometric SnO_x thin films deposited by reactive sputtering with the impedance control, *J. Appl. Phys.* **127** 185703 (2020).

[11] J. Jia, A. Takaya, T. Yonezawa, K. Yamasaki, H. Nakazawa, Y. Shigesato, Carrier densities of Sn-doped In_2O_3 nanoparticles and their effect on X-ray photoelectron emission, *J. Appl. Phys.* **125** 245303 (2019).

[12] V. Pačebutas, G. Aleksejenko, A. Krotkus, J. W. Ager III, W. Walukiewicz, Hai Lu, and W. J. Schaff, Optical bleaching effect in InN epitaxial layers, *Appl. Phys. Lett.* **88**, 191109 (2006).

[13] S. Tiwari, E. Kioupakis, J. Menendez, and F. Giustino, Unified theory of optical absorption and luminescence including both direct and phonon-assisted process, *Phys. Rev. B* **109**, 195127 (2024).

[14] S. A. Sato, Y. Shinohara, T. Otobe, K. Yabana, Dielectric response of laser-excited silicon at finite electron temperature, *Phys. Rev. B* **90**, 174303 (2014).

[15] M. Schultze, K. Ramasesha, C. D. Pemmaraju, S. A. Sato, D. Whitmore, A. Gandman, J. S. Prell, L. J. Borja, D. Prendergast, K. Yabana, D. M. Neumark, S. R. Leone, Attosecond band-gap dynamics in silicon, *Science* **346**, 1348 (2014).

[16] J. Jia, N. Oka, Y. Shigesato, Direct observation of the band gap shrinkage in amorphous $\text{In}_2\text{O}_3\text{–ZnO}$ thin films, *J. Phys. Appl.* **113**, 163702 (2013).

[17] F. Chen, A. N. Cartwright, H. Lu, and W. J. Schaff, Time-resolved spectroscopy of recombination and relaxation dynamics in InN, *Appl. Phys. Lett.* **83**, 4984 (2003).

[18] S. Sun, Y. Wen, S. Guol, H. Lee, S. Gwo, and C. Sun, Observation of femtosecond carrier thermalization time in indium nitride, *J. Appl. Phys.* **103**, 123513 (2008).

[19] W. Paszkowicz, X-ray powder diffraction data for indium nitride, *Powder Diffraction*, **14**, 258 (1999). DOI: <https://doi.org/10.1017/S0885715600010630>.

[20] J. Kuzmík, C. Fleury, A. Adikimenakis, D. Gregušová, M. Čapajna, E. Dobročka, Š. Haščík, M. Kučera, R. Kúdela, M. Androulidaki, D. Pogany, A. Georgakilas, Current conduction mechanism and electrical breakdown in InN grown on GaN, *Appl. Phys. Lett.* **110**, 232103 (2017).

[21] J. Menéndez, C. D. Poweleit, and S. E. Tilton, Temperature dependent photoluminescence in Ge: Experiment and theory, *Phys. Rev. B* **101**, 195204 (2020).

[22] G. Kresse and J. Furthmüller, Efficient iterative schemes for ab initio total-energy calculations using a plane-wave basis set, *Phys. Rev. B* **54**, 11169 (1996).

[23] G. Kresse and D. Joubert, From ultrasoft pseudopotentials to the projector augmented-wave method, *Phys. Rev. B* **59**, 1758 (1999).

[24] C. Rödl, J. Furthmüller, J. R. Suckert, V. Armuzza, F. Bechstedt, and S. Botti, Accurate electronic and optical properties of hexagonal germanium for optoelectronic applications, *Phys. Rev. Materials* **3**, 034602 (2019).

[25] J. Furthmüller, P. H. Hahn, F. Fuchs, and F. Bechstedt, Band structures and optical spectra of InN polymorphs: Influence of quasiparticle and excitonic effects, *Phys. Rev. B* **72**, 205106 (2005).

[26] V. Yu. Davydov, A.A. Klochikhin, R.P. Seisyan, V.V. Emtsev, S.V. Ivanov, F. Bechstedt, J. Furthmüller, H. Harima, A.V. Mudryi, J. Aderhold, O. Semchinova, J. Graul, Absorption and emission of hexagonal InN: Evidence of narrow fundamental band gap, *Phys. Status Solidi B* **229**, R3 (2002).

[27] E. Burstein, Anomalous optical absorption limit in InSb, *Phys. Rev.* **93**, 632 (1954); T. S. Moss, The interpretation of the properties of indium antimonide, *Proc. Phys. Soc. B* **67**, 775 (1954).

[28] E. O. Kane, Band structure of indium antimonide, *J. Phys. Chem. Solids*, **1**, 249 (1957).

[29] J. Wu, W. Walukiewicz, W. Shan, K. M. Yu, J. W. Ager, E. E. Haller, H. Lu, and W. J. Schaff, Effects of the narrow band gap on the properties of InN, *Phys. Rev. B* **66**, 201403(R) (2002).

[30] S. P. Fu, and Y. F. Chen, Effective mass of InN epilayers, *Appl. Phys. Lett.* **85**, 1523 (2004).

[31] C. Xu, N. S. Fernando, S. Zollner, J. Kouvetsakis, and J. Menéndez, Observation of phase-filling singularities in the optical dielectric function of highly doped *n*-type Ge, *Phys. Rev. Lett.* **118**, 267402 (2017).

[32] I. Gorczyca, J. Plesiewicz, L. Dmowski, T. Suski, N. E. Christensen, A. Svane, C. S. Gallinat, G. Koblmüller, J. S. Speck, Electronic structure and effective masses of InN under pressure, *J. Appl. Phys.* **104**, 013704 (2008).

[33] Y. Su, Y. Wen, H. Lee, S. Gwo, and C. Sun, Observation of sub-100 femtosecond electron cooling time in InN, *Appl. Phys. Lett.* **96**, 052108 (2010).

[34] Y. Wen, C. Chen, C. Shen, S. Gwo, and C. Sun, Ultrafast carrier thermalization in InN, *Appl. Phys. Lett.* **89**, 232114 (2006).

[35] N. Del Fatti, C. Voisin, M. Achermann, S. Tzortzakis, D. Christofilos, and F. Vallee, Nonequilibrium electron dynamics in noble metals, *Phys. Rev. B* **61**, 16956 (2000).

[36] C. K. Sun, F. Vallée, L. Acioli, E. P. Ippen, and J. G. Fujimoto, Femtosecond investigation of electron thermalization in gold, *Phys. Rev. B* **48**, 12365 (1993).

[37] M. I. Kaganov, I. M. Lifshitz, and L. V. Tanatarov, Relaxation between Electrons and the Crystalline Lattice, *Zh. Eksp. Teor. Fiz.* **31**, 232 (1957) [Sov. Phys. JETP 4, 173 (1957)].

[38] I. Barin, O. Knacke, O. Kubaschewski, Thermo dynamical properties of inorganic substances, (Springer-Verlag, Berlin, 1977).

[39] J. Singleton, Band theory and electronic properties of solids, (Oxford university press, 2001).

[40] V. E. Alexopoulou, A. P. Markopoulos, A Critical Assessment Regarding Two-Temperature Models: An Investigation of the Different Forms of Two-Temperature Models, the Various Ultrashort Pulsed Laser Models and Computational Methods, *Archives of Computational Methods in Engineering* **31**, 93 (2024).

[41] C. D. Aeaby, and A. Ray, Two-temperature model for ultrafast melting of Au-based bimetallic films interacting with single-pulse femtosecond laser: Theoretical study of damage threshold, *Phys. Rev. B* **107**, 195402 (2023).

[42] Z. Lin, and L. V. Zhigilei, Electron-phonon coupling and electron heat capacity of metals under conditions of strong electron-phonon nonequilibrium, *Phys. Rev. B* **77**, 075133 (2008).

[43] H. E. Elsayed-Ali, T. B. Norris, M. A. Pessot, and G. A. Mourou, Time-resolved observation of electron-phonon relaxation in copper, *Phys. Rev. B* **58**, 1212 (1987).

[44] C. Kittel, *Introduction to Solid State Physics* (8 ed.). United States of America: John Wiley & Sons, Inc. p. 146. ISBN 978-0-471-41526-8 (2005).

V. ACKNOWLEDGMENTS

J. Jia acknowledges the funding support from JSPS KAKENHI Grant-in-Aid for Scientific Research (B) (Grant No. 25K01862) and from Waseda University Grant for Special Research Projects (Project No. 2025C—157). R. Nakazawa, K. Fukutani, and S. Kera acknowledges support from JSPS KAKENHI Grant-in-Aid for JSPS Fellows (Grant No. 25KJ0391).

VI. AUTHOR CONTRIBUTIONS

JJ initiated and formulated the research idea. JJ and TM fabricated the InN film. MK and YS conducted transmittance and reflectance experiments. JJ and TY developed the pump-probe measurement system and collected the experimental data. RN, KF and SK carried out the HS-UPS measurements. JJ wrote/revised the manuscript. All authors reviewed the manuscript.

VII. DATA AVAILABILITY

The data that support the findings of this study are available from the corresponding author, JJ, upon reasonable request.

VIII. COMPETING INTERESTS

The authors declare no competing interests.